MICROSTRUCTURE AND MECHANICAL PROPERTIES OF AA6056 FRICTION STIR WELDED PLATE

[1]H.J. McQueen, [2]M. Cabibbo, [2]E. Evangelista, [2]S. Spigarelli, [3]M. Di Paola, [3]A. Falchero
[1]Mechanical Engineering, Concordia University, Montreal, H3G IM8, Quebec, Canada
[2]Dip. Meccanica, Università Politecnica delle Marche, Ancona, Italy,
[3]Alenia Aeronautica, Torino, Italy

Abstract

The microstructure and mechanical properties of a friction stir welded AA6056-T6 aluminum alloy plate were investigated by using polarized optical and transmission electron microscopy techniques. The microstructure revealed different grain morphologies in the thermo-mechanically affected zones, in proximity of the weld nugget; as the advancing side had fairly elongated, bent grains, whilst the broader retreating side had elongated grains whose width is narrower compared to the advancing side. On both sides, the thermo-mechanical affected zones showed a process of grain subdivision due to shear strain and temperature increase on approaching the nugget zone. Along with overaged precipitates in both thermo-mechanically affected zones, β" and β' particles were detected only within the retreating side. Tensile tests showed yield and ultimate strength slightly lower across the weld compared to the parent material; this difference resulted in a reduction in ductility of the weld region.

Riassunto

Il lavoro di ricerca, oggetto del presente lavoro, presenta i risultati relativi alle indagini microstrutturali mediante microscopia ottica in luce polarizzata e microscopia elettronica in trasmissione su un giunto in AA6056-T6, realizzato mediante *friction stir welding*. La zona termo-meccanicamente alterata mostra una morfologia a grani ben diversa da quella evidenziata in corrispondenza del nugget. Inoltre è stata documentata una asimetria microstrutturale tra il lato di avanzamento del pin, in rotazione rispetto ai laminati da saldare, e quello opposto. La regione di avanzamento mostra grani allungati ed estremamente curvati, mentre la zona opposta, rispetto al nugget, presenta grani allungati ma molto più sottili rispetto al lato di avanzamento (maggiore rapporto tra lunghezza ed ampiezza). In entrambi i lati i grani sono, comunque, soggetti a frammentazione il che è dovuto a processi di deformazione plastica ed escursione termica durante la saldatura, sebbene fenomeni di precipitazione di fasi indurenti quali β" e β' siano stati rivelati solo all'interno della zona opposta a quella di avanzamento.
Prove di trazione hanno mostrato una resistenza a snervamento e a rottura leggermente più basse in corrispondenza della zona saldata, rispetto a quelle del materiale base, questo indica valori di duttilità leggermente inferiori in corrispondenza del giunto di saldatura.

INTRODUCTION

The major advantages of friction stir welding (FSW in aluminum alloys, when compared to conventional fusion welds, are primarily the elimination of cracking and evaporative loss of alloying elements. This is due to the solid-state joining and a weld zone with fine worked or recrystallized grain structure generated by stirring and forging during FSW [1]. During welding, temperatures remaining below the melting point, result in a low shrinkage phenomenon and excellent mechanical properties, together with reduction of residual stress within the welded zone [2-13]. Mechanical properties of the FSW joint are quite good and fatigue properties are practically the same as the parent metal [1]. Generally, tensile failures occur well away from the nugget [1,2].

To date, the major application fields of FSW are marine industries (ship sections, hulls, structures), aerospace industry (fuselages, wings, fuel tanks), railway industry (high speed trains, carriages), automotive industry (chassis, wheel rims, space frames, truck bodies) motorcycle frames and other sectors, such as electrical and refrigeration [1].

Due to the combined effect of the tooling, FSW produces five different microstructure zones: the nugget in the centre of the weld where the pin has passed, a shoulder contact zone on the top surface, thermo-mechanically affected zones (TMAZ) that are immediately on each side of the nugget, heat affected zones (HAZ) adjacent to the TMAZ that experiences a thermal cycle but no a mechanical shearing, and the unaffected parent material [4,5,7,14-18]. FSW produces an asymmetric microstructure in which the advancing and retreating sides experience different strain levels and thermal cycles [3,16]. Material on the advancing side (rotation opposed to plate motion) experiences more shear than the retreating does [3]. The closer the material to the tool, the higher is the deformation and temperature gradients to which it is subjected. This implies an effective deformation rate higher in the advancing side than in the retreating, resulting in different stress, flow and temperature cycles [16]. Moreover, almost all the metal form in front of the tools isheared to the retreating side creating a much broader flow band than on the advancing. In addition to the grain and substructure evolution during the severe thermo-mechanical conditions imposed by FSW, the various thermal cycles in the different weld zones induce different precipitate distributions within each zone [12-14].

The present paper reports a microstructure and mechanical study on a AA6056 T6, FSW plate. The microstructure inspections focused on the asymmetric aspects within the TMAZ between the advancing and retreating side of the weld, especially in terms of grain morphology and secondary particle alteration. Tensile and hardness tests were carried out across the weld nugget and compared to the parent material.

EXPERIMENTAL METHODS

FSW has been carried out by Alenia Aeronautica (Torino) as a bead-on-plate weld. The welding was performed under pin load control at a rotational speed of 1800 rpm and an angle of 3¡ respect to the plate axis; plate translational speed was of 15 mm/s. The tool consisted of a 18 mm diameter flat, scrolled shoulder and truncated cone pin, whose tip size was of 1.8 mm. The 10-mm thick welded plate was AA6056 (1.1 Mg, 0.65 Si, 0.23 Cr, 0.15 Mn, Al bal., in wt.%) in the T6 condition.

Weld cross section and middle-transverse section of the weld were ground, polished and anodized (a solution of 4% fluoro-boridic acid in ethanol at 25V for 120s) for polarized optical microscopy (POM) inspections. The grain structure of the different welded zones (nugget, TMAZ, HAZ) and the parent material was characterized by POM. Statistical evaluation of grain mean size and aspect ratio was carried out by image analysis software.

Sheets for transmission electron microscopy (TEM), were extracted from the middle-longitudinal section along the welded zone. Various weld locations were selected in the attempt to follow the microstructure changes, from the parent material, to the nugget on both advancing and retreating side. Care was taken for the correspondence of locations to the hardness profile along the weld. Sheets were ground to 200 mm thickness, chemically polished to 70 mm, punched as 3-mm discs. A Tenupol-5 twin jet electro-polisher was used to produce electron transparent sections using a solution of 30% nitric acid in methanol at -35¡C and 18V. TEM inspections were carried out on a Philips CM200 operating at 200kV and equipped with a double tilt stage. Boundary misorientation has been measured by using the Kikuchi pattern method [19].

Vickers micro-hardness was carried out with a 100gf load and 15s dwell time; data were acquired along the longitudinal section at the middle thickness of the weld and each data point averages some 5 different measurements, the distance apart being 0,25 mm. Tensile tests were performed on a 250 kN servo-hydraulic machine operated in ram displacement control at room temperature and with a nominal strain rate of $2\Diamond10^{-1}s^{-1}$. A computer-based data acquisition system was used to control machine operation and data recording. Two stets of specimens were extracted, one from across the welded region, another far away from the welded zone, within the parent material. Both sets of test-pieces were extracted along the transverse direction, in order to avoid textural inhomogeneities.

RESULTS

Fig. 1 shows panoramic views of the cross section and transversal middle-thickness section of the welded plate. Material moves upwards and the tool spins counter clockwise, thus the advancing side is on the left and retreating on the right. There are seven different regions across the weld, three on each side of the nugget (parent material, HAZ, TMAZ). From Fig. 1 (b), (d) it is clear that there is

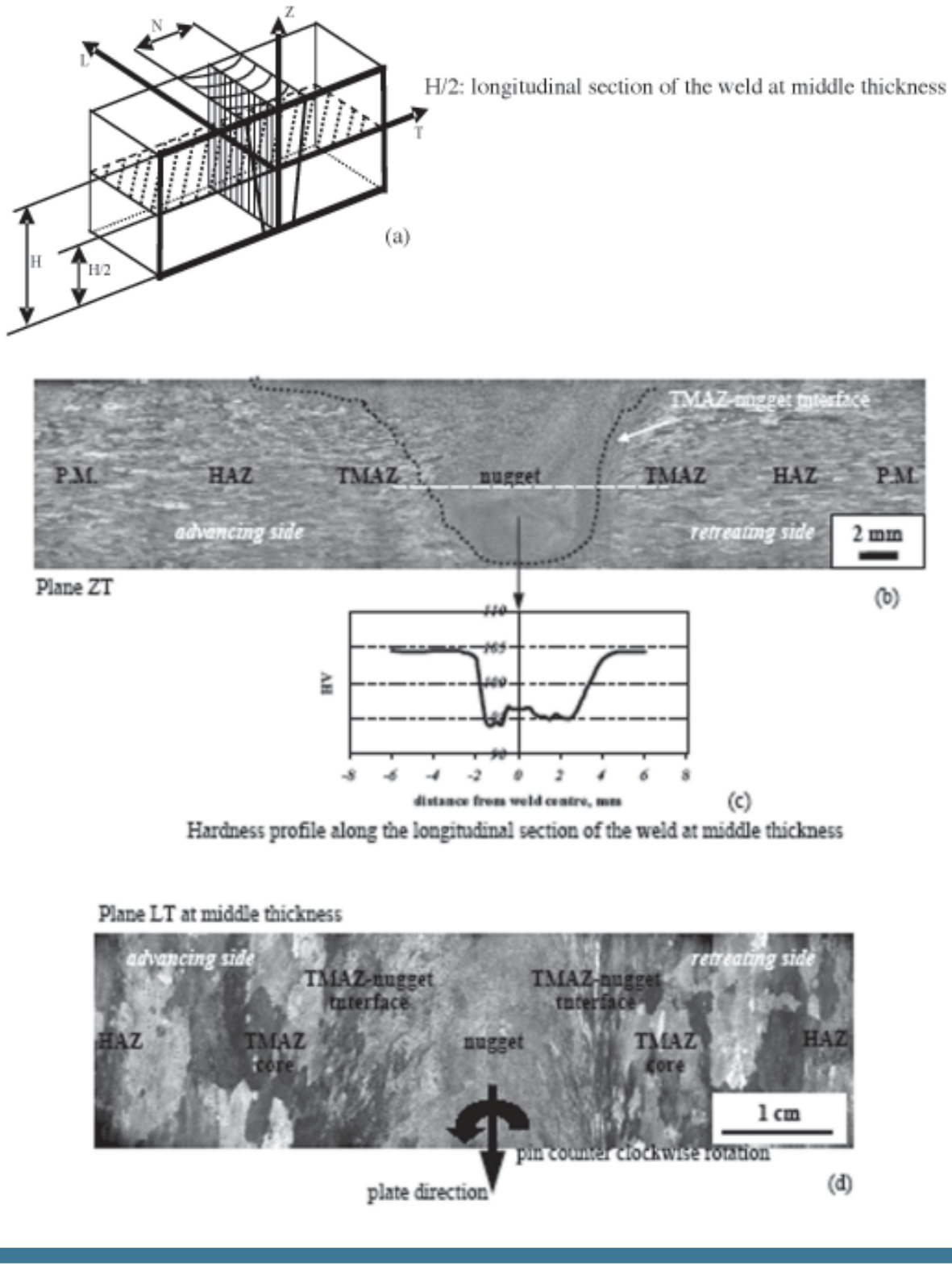

Fig. 1: Coordinate system scheme (a); polarized optical micrographs (POM) of the cross section (b), and longitudinal section at middle thickness (d) across the friction stir weld. The major zones (HAZ, TMAZ, nugget) of which the weld is composed are labeled. A micro-hardness profile, of same scale as (a), is reported in (c), showing a double, but not symmetrical, minimum in the TMAZ.

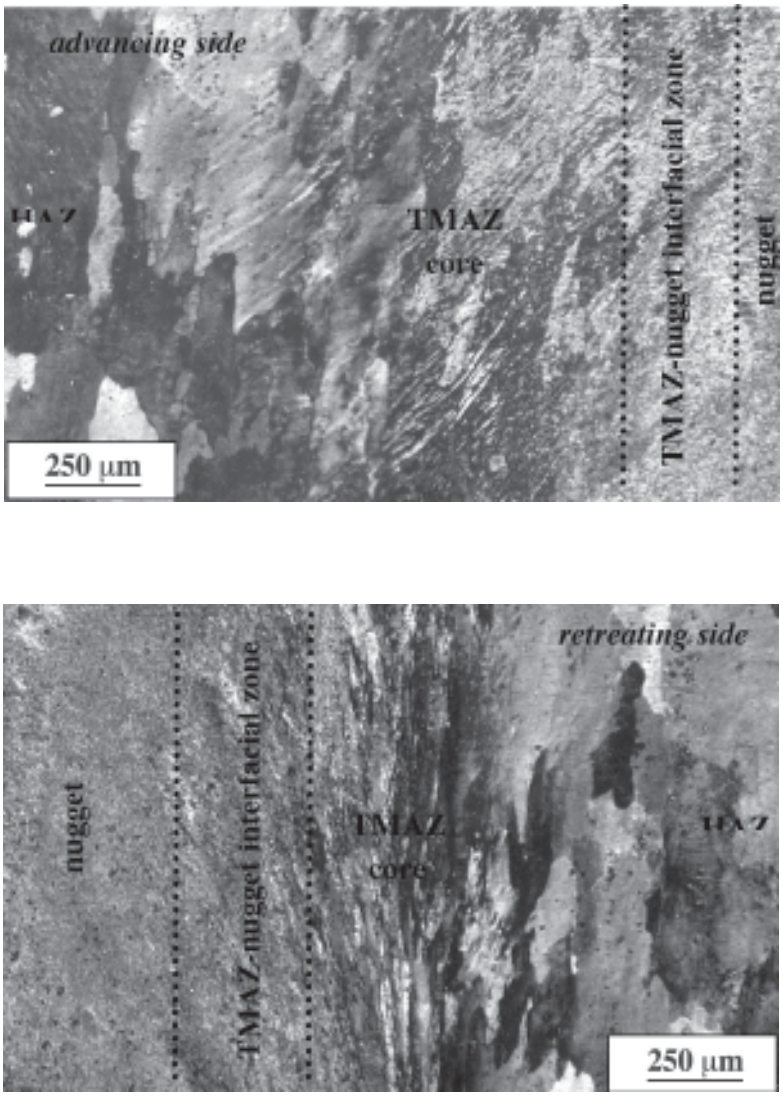

Fig. 2: POM of the advancing side (a), and retreating side (b), showing the deformed grain structure within the TMAZ core and the wide interfacial region (b) between TMAZ and nugget, with alternating layers of elongated grains and fine crystallites.

not a smooth narrow interface between nugget and TMAZ on either side. This indicates material is bulged from advancing side and both swept and bulged from retreating side to fill in behind the pin. In Fig. 2 (a) and (b), POM documents the different microstructural zones from the parent material to the nugget zone, on the advancing and retreating sides. In both TMAZ, the grains are bent upwards indicating additional displacement, relative to parent plates, caused by the advancing pin somewhat similar to the flow around a punch, or hardness indenter. On the advancing side, grains in the TMAZ have bulged only a little into the region behind the pin, leaving a sharp interface between the TMAZ and nugget. On the retreating side, such flow is greater because the rotating tool shears metal from before it to that side. Moreover, the additional sweeping of material into the region behind the pin results in a very irregular interface between elongated grains and the equiaxed nugget. The TMAZ-nugget interface zone is very wide, having alternating layers of elongated grains with fine cells and of crystallites with larger diameter. The micro-hardness profile, along the middle section of the weld is reported in Fig. 1 (c). The frictional heat results in a minimum of the hardness because of the growth and coarsening of the T6 strengthening precipitates.

TEM micrographs of the nugget, at two different magnifications in (Fig. 3 (a,b)), exhibit the structure where the pin has passed. The fine equiaxed crystallite structure with average size of 12 mm in diameter is finer by a factor of roughly 40 than the 450 mm grains of the parent material. Kikuchi diffraction pattern analyses, performed by TEM, revealed these boundaries to be mostly high-angle, about 80% HAB. On both sides of the nugget in the TMAZ cores (Fig. 3 (c,f)), grains are elongated and bent similarly, both being 350 mm in equivalent diameter with an aspect ratio rising from 3 to 11 on approaching the nugget zone. Crystallites have grown by dynamic recovery (DRV) because of the higher temperature or lower strain rate than in the TMAZ core, with some static recovery (SRV) later. The alternating layers of crystallites and elongated grains with cells indicate there has been no discontinuous recrystallization. Moreover, there was no evidence of growth by boundary migration from lower density nugget layers to more deformed cell layers.

In the region close to the pin, i.e. the sharp interface zone between the TMAZ and nugget, the grain structure appears as elongated bands of fine crystallites which are quite similar to the ones observed within the nugget region. The core of advancing side TMAZ, characterized by having a large fraction of high-angle boundaries (HABs), is the result of both shear strain and temperature

increasing as the material approaches the pin. In comparison to the advancing side, the retreating side TMAZ is wider due to the tool rotation causing the material ahead of the pin to displace to the right-hand side. This process is accompanied by a continuous decrease in the strain of the rotated material, with distance from the rotating pin. Furthermore, the TMAZ band closest to the nugget appears as a mixture of fine crystallites, approaching the cell dimension in the elongated grains, as already noted for the advancing side TMAZ-nugget interface. From TMAZ-nugget interface, Fig. 4 shows the intersection of a

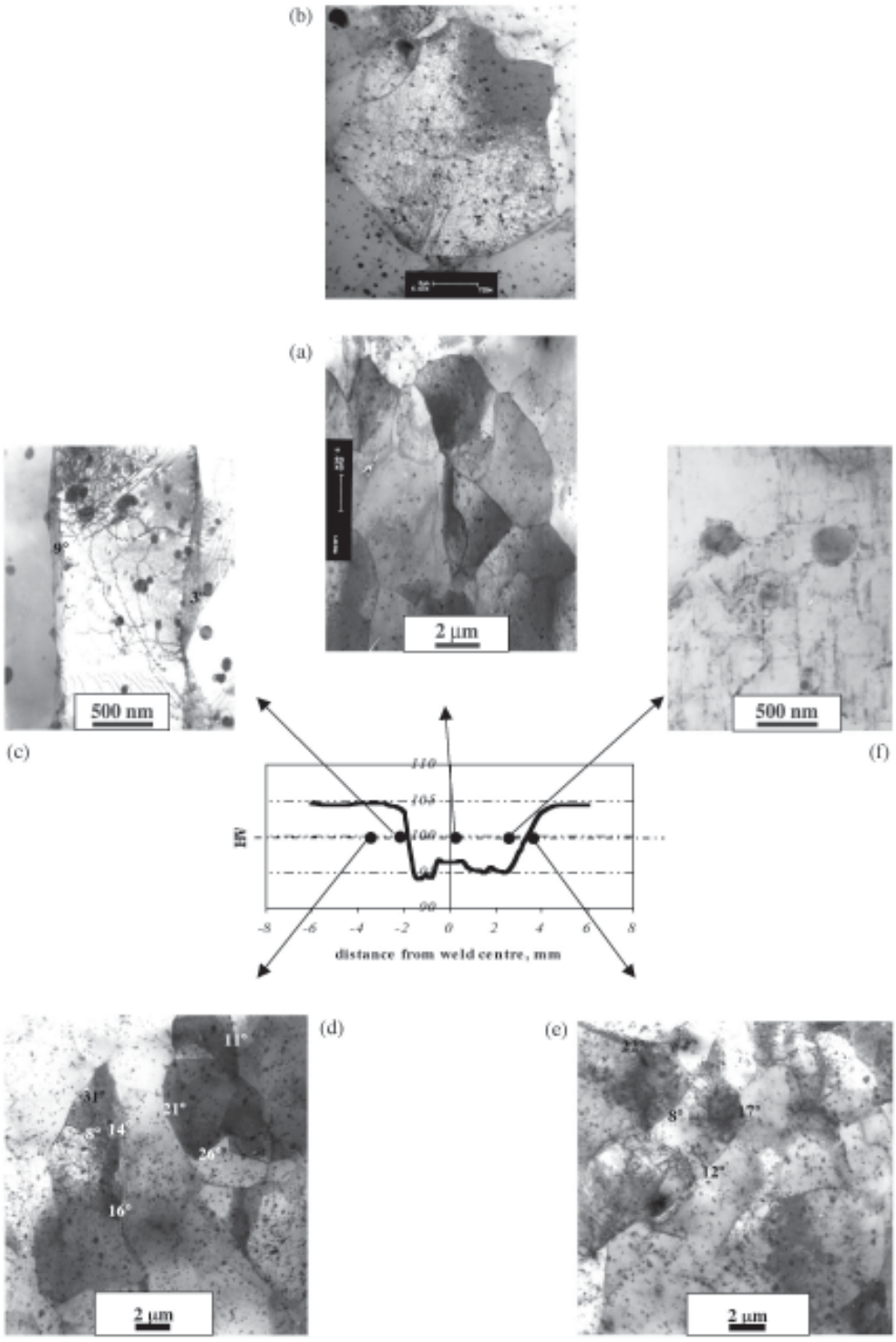

Fig. 3: Transmission electron micrographs (TEM) showing the microstructure of the nugget at two different magnifications, 3800x (a), 6600x (b), and TMAZ in the advancing side (c,d), and retreating side (e,f) at different locations.

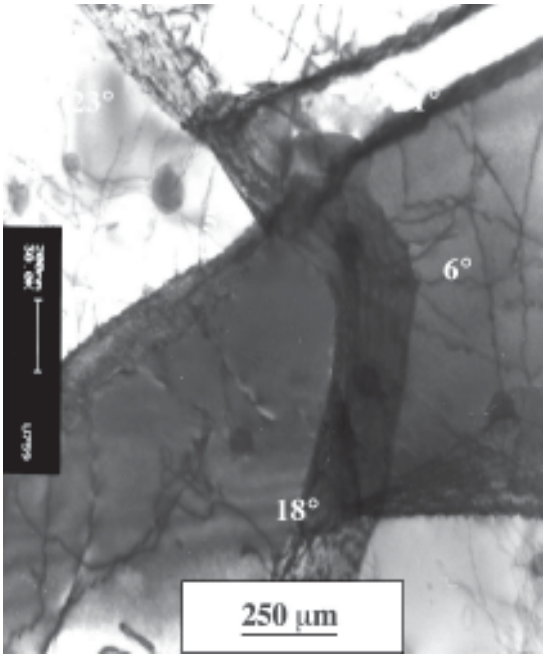

Fig. 4: Example of microstructure detail of two almost high-angle boundaries crossed by one low-angle boundary observed in the advancing side TMAZ-nugget interface zone.

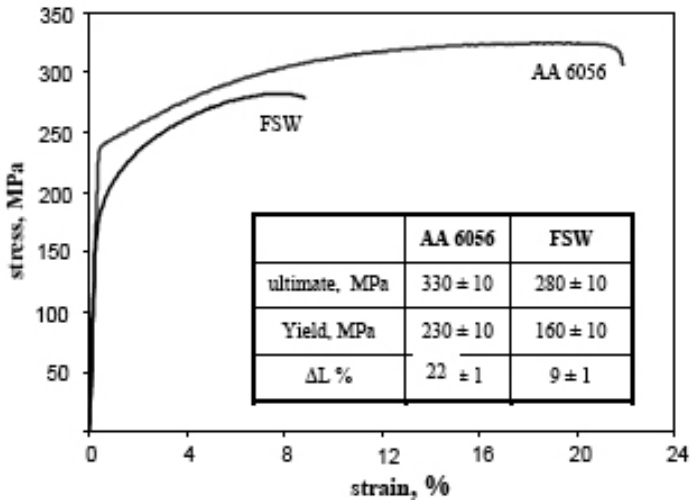

Fig. 5: Tensile curves of FSW and parent material. Curves constitute an average over 4 different tests. FSW test-specimens were cut along the middle-longitudinal section across the weld, base alloy test-pieces maintain the same orientation to the weld, to avoid textural contributions. Average ultimate, yield strength and ductility (DL, %) are reported in the graph insert.

low-angle boundary (LAB) and a strain induced high-angle boundary (HAB) that would not be possible with an original grain boundary. Diffuse dislocation interactions with fine particles and Frank network dislocations inside subgrains, are also observed at the TMAZ-nugget interface, on the retreating side. They are believed to form during the thermal quench from the high welding temperature to the room temperature.

An interesting aspect is the asymmetric precipitation sequence occurring on the retreating side with respect to the advancing side. The advancing side has solely large precipitates (> 400-500 nm) that might come from overaging during the passage of the pin (Fig. 3 (c)). Beside coarse particles, the retreating side is characterized by fine rounded particles (less than 300 nm) and finer needle-like precipitates (less than 200nm long with one-tenth the width) that are G.P. zones and b' (Fig. 3 (f)). These fine particles result in slightly higher hardness values in the retreating TMAZ-nugget interface (Fig. 1). In both sides the dislocation density within the grains is rather high. Quite a number of dislocations pinned by secondary phase particles were observed, especially in the retreating side. The grain structure of the HAZ is similar to that of the parent material. The mean grain size was 470 mm and 390 mm in the advancing and retreating side, respectively, with a common aspect ration of about 2.5 against 2.2 of the parent material. This slight increase in aspect ratio is quite little compared to change in the TMAZ core and confirms that the HAZ has deformed very slightly at the most.

Fig. 5 shows the tensile curves carried out on specimens from across the welding zone and from the parent material. Compared to the base alloy, the ductility of the joint is near 40%, but the ultimate strength is about 90% (280 MPa relative to 330 MPa) and the yield strength is about 66% (160 to 230 MPa).

DISCUSSION

The large scale pattern of grain flow is similar to that observed in other studies, being in agreement with some reports [3,6,7,10-15,20,21], and disagreement with others [5,22-27]. The flow in the retreating side seems to be much greater and broader than on the advancing side. If the material flow would have been induced by a non-rotating indenter, there would be equal flow on both sides, somewhat like the cross-section of a tubular impact extrusion; here grains are bent upwards from the parent plates that provide the die walls. The rotation of the tool induces a narrow shear

strain gradient (Figs. 1, 2(a)), and thermal spike generated on the advancing side. The tool rotation carries much material in front of it, towards the retreating side, producing a higher flow rate (Figs. 1, 2). The heat in that transported metal helps to develop a much broader temperature gradient that facilitates the more massive plastic deformation. Despite difference in the plastic zone width, the degree of strain in the TMAZ cores is roughly the same based on the change in aspect ratio of the grains. With allowance for differences in parent metal and welding conditions, the present anisotropic microstructures are consistent with microscopic, thermal and flow studies and simulations reported for several aluminum alloys and stainless steels [3,5,6,8,10,12,13,16-18,21-26]. Cho *et al.* [3] found that the effective stress was highest in the stirred zone and higher on the advancing side than on the retreating side; the mean stress was compressive ahead of the tool and tensile behind the tool (Fig. 1). Reynolds and co-workers [28,29] documented for AA2024 a banded structure within the TMAZ and mixed banded and almost equiaxed crystallites at the TMAZ-nugget interface, in agreement with the present microstructures (Fig. 2) and changes in mechanical strength (Fig. 5).

The sharp drop, on the advancing side, in the hardness profile (Fig. 1 (c)), supports a narrow temperature spike as suggested above. The very low hardness zone is related to the disappearance of G.P. zones and formation of overaged precipitates (Fig. 3 (c)). The slightly higher hardness in the retreating TMAZ is due to a broader temperature gradient resulting in less dissolution and overaging (Fig. 3 (f)). The higher hardness in the nugget is related to complete solution and new precipitation in this slowest cooling zone; this is counteracted by the additional softening relative to the TMAZ due to substructure coarsening. As regard to the different precipitation populations in the TMAZ between the advancing and retreating side, several studies attempted to correlate the temperature cycles and strain rate to a possible induced secondary phase precipitation sequence [5,12,16-18,27-29]. Yang et al. [22] measured the peak temperatures for three different FSW tool speeds in two 2000 series alloys. In their paper, they reported a lower particle fraction, size and density in the advancing side TMAZ in similarity to behavior detected in our inspections. A study on a AA2024 by Norman et al. [5] reported temperature peaks of 450-500¡C and 450-350¡C for the nugget and TMAZ, respectively; on this basis they proposed only partial dissolution in the TMAZ and complete solution of particles within the nugget, possibly followed by precipitation during cooling [5,30-33].

The nugget is formed to a limited extent by the material from each side of the pin flowing into the region it is vacating as a result of lateral constraints by the parent plates. The region is mainly filled by the hottest metal in the broad retreating side flow zone, being swept in by the pin rotation. This is confirmed by the wide feathery interface of mixed elongated and equiaxed layers (Fig. 2 (b)). The strain rate declines gradually to zero as the pin moves further away, before cooling takes place. The substructure increases in dimensions by dynamic recovery (DRV), as confirmed by the 12 mm crystallite size compared to 2 mm subgrains in the TMAZ (Fig. 3 (d),(e)). Some static recovery (SRV) occurs after all straining has stopped, but it is much less effective than DRV.

The TMAZ can best be understood from the theory of geometric dynamic recrystallization (gDRX) [25,26,32-37]. During steady state straining (in narrow bands) at constant temperature and strain rate, the subgrains remain equiaxed as the grains elongate developing serrated boundaries [25,26]. Due to the greater grain boundary area, the density of HAB increases and many subgrains have several high-angle facets [26,32]. These small cellular regions are renamed crystallites, being intermediate between subgrains and grains. In the core of the TMAZ, the grains elongate but never become thinner than about two subgrain diameters [36,37]. Due to the mobility of grain boundaries as they absorb intersecting sub-boundaries, serrations in neighboring grain boundaries impinge. This pinches off the grain making it shorter but, at the same time, making the neighbors thicker. In POM, the elongated regions from an initial grain are still evident due to similar texture. As strain rate decreases in the nugget region, the crystallites grow larger by rearrangement of the sub-boundaries as occurs during creep tests when the strain rate is changed [38,39]. The time at high temperature after straining is too short for discontinuous static recrystallization (dSRX) to take place even at interfaces between the equiaxed and elongated regions with greater sub-structure density.

In similarity to this, Su et al. [11] have reported in AA7050 the transformation of elongated grains with 1-2um cells in the TMAZ into 1-4 um equiaxed structure with many HAB in the nugget. They proposed that the growth and the creation of HAB occurred by some cell walls absorbing dislocations; they failed to consider rearrangement of the GB from the TMAZ through the gDRX mechanism. In one part of the nugget of AA2024, Norman et al. [5] observed 6.3
um crystallites (63% HAB)coming from about 3.1 um cells (73% HAB) in the TMAZ in similarity to the present: however in the nugget center, they suggest that the 2.4 um grains (85% HAB) were produced by discontinuous DRX from the TMAZ.

Prangnell and colleagues [40], have shown that the crystallite size in the nugget is consistent with structures developed in torsion to the same strain at equivalent temperatures and strain rates. Jata and Semiatin [41] found nugget crystallite size consistent with torsion subgrains in an Al-Li alloy [42]. Because of the refined crystallite structure developed and despite the diminished precipitation hardening, the FSW weld quality is far higher than conventional fusion welding as confirmed by the results of the mechanical tests.

SUMMARY

The microstructure of a FSW AA6056-T6 plate was investigated by POM and TEM. The grain structure can be divided into several major regions: i) fine equiaxed crystallites in the nugget at the weld centre, ii) highly elongated grains with very small cells in the broad retreating side TMAZ and in the narrow advancing side, and iii) slightly elongated coarse grains in the HAZ and the parent material. Strain rate and temperature gradients are much steeper in the advancing side than in the retreating. The nugget is defined by large crystallites formed by sub-boundary rearrangement from fine subgrains swept in from the TMAZ due to high temperature and low strain rate. Precipitation distribution was quite different from the needle-like T6 particles in the parent material with some coarsening in the HAZ. Solely in the retreating side TMAZ a bimodal particle population was detected being composed of remaining aged precipitates together with coarse incoherent b-Mg_2Si particles. The advancing side TMAZ shows a narrow zone of overaged precipitates only. The hardness profile is lowest in the advancing side TMAZ, slightly higher in the retreating side TMAZ and higher in the nugget where greater dissolution was accompanied by re-precipitation. Mechanical properties of the welded region were quite good, the ultimate being 90% and yield strength 66% of the values in the base alloy.

LEGENDA

DRV: dynamic recovery
dSRX: discontinuous static recrystallization
FSW: friction stir welding
GB: grain boundary
gDRX: geometric dynamic recrystallization
HAB: high-angle boundary
HAZ: heat affected zone
LAB: low-angle boundary
PM: parent material
POM: polarized optical microscopy
SRV: static recovery
TEM: Transmission electron microscopy
TMAZ: thermo-mechanically affected zone

ACKNOWLEDGMENTS

The authors wish to acknowledge D. Ciccarelli for POM specimen preparation.

REFERENCES

1. TALAT lecture 4410, Friction Stir Welding, TWI, 1999.
2. W.M. Thomas, E.D. Nicholas, Mater. Design, 1997, 18, 269.
3. J.-H. Cho, D.E. Boyce, P.R. Dawson, Mater. Sci. Eng. A, 2005, 398, 146.
4. M.A. Sutton, A.P. Reynolds, B. Yang, R. Taylor, Mater. Sci. Eng. A, 2003, 354, 6.
5. A.F. Norman, I. Brough, P.B. Prangnell, Mater. Sci. Forum, 2000, 331-337, 1713.
6. H.G. Salem, Scripta Mater., 2003, 49, 1103.
7. S. Benavides, Y. Li, L.E. Murr, Ultrafine grain structure in the friction-stir welding of aluminium alloy 2024 at low temperatures, Conf. Proc. of Ultrafine grained materials, Eds. R.S. Mishra, S.L. Semiatin, C. Suryanarayana, N.N. Thadhani, T.C. Lowe, TMS, 2000, 155.
8. M. Boz, A. Kurt, Mater. Design, 2004, 25, 342.
9. W.M. Thomas, Friction stir welding International Patent application, No. PCT/GB92 Patent application No. 9125978.8, 1991.
10. B. Heinz, B. Skrotzki, G. Eggeler, Mater. Sci. Forum, 2000, 331-337, 1757.
11. J.-Q. Su, T.W. Nelson, R. Mishra, M. Mahoney, Acta Mater., 2003, 51, 713.
12. Y.S. Sato, H. Kokawa, M. Enomoto, S. Jogan, Metall. Mater. Trans. A, 1999, 30, 2429.
13. C. Genevois, A. Deschamps, A. Denquin, B. Doisneau-cottignies, Acta Mater., 2005, 53, 2447.
14. G. Liu, L.E. Murr, C.-S. Niou, J.C. McClure, F.R. Vega, Scripta Mater., 1997, 37, 355.
15. R.W. Fonda, J.F. Bingert, K.J. Colligan, Scripta Mater., 2004, 51, 243.
16. C. M. Chen, R. Kovacevic, Int. J. Mach. Tools Man., 2003, 43, 1319.
17. W.D. Lockwood, A.P. Reynolds, Mater. Sci. Eng. A, 2003, 339, 35.
18. Ø. Frigaard, Ø. Grong, O.T. Midling, Metall. Mater. Trans. A, 2001, 32, 1189.
19. Q. Liu, Ultramicroscopy, 1992, 41, 317
20. Y. Li, L.E. Murr, J.C. McClure, Mater. Sci. Eng. A, 1999, 271, 213.
21. P.B. Prangnell, C.P. Heason, Grain structure

formation during friction stir welding observed by the 'stop action technique', Acta Mater., 2005, 53, 3179.

22. K.V. Jata, K.K. Sankaran, J.J. Rushau, Metall. Mater. Trans. A, 2000, 31, 2181.
23. Kh.A.A. Hassan, A.F. Norman, D.A. Price, P.B. Prangnell, Acta Mater.,2003, 51, 1923.
24. H.J. McQueen, Mater. Sci. Eng. A, 1988, 101, 149.
25. E.V. Konopleva, H.J. McQueen, E. Evangelista, Mater. Charact., 1995, 34, 251.
26. H.J. McQueen, W. Blum, Mater. Sci. Eng. A, 2000, 290, 95.
27. A.K. Gupta, D.J. Lloyd, S.A. Court, Mater. Sci. Eng. A, 2001, 316, 11.
28. M. Cabibbo, S. Spigarelli, E. Evangelista, Mater. Charact., 2003, 49, 3, 193.
29. M. Cabibbo, E. Evangelista, M. Vedani, Metall. Mater. Trans. A, 2004, 35, 293.
30. A.P. Reynolds, W. Tang, T. Gnaupel-Herold, H. Prask, Scipta Mater., 2003, 48, 1289.
31. M.W. Mahoney, C.G. Rhodes, J.G. Flintoff, R.A. Spurling, W.H. Bingel, Metall. Mater. Trans. A, 1998, 29, 1955.
32. H.J. McQueen, M.E. Kassner, Scripta Mater. 51 (2004) 461-465.
33. B. Yang, J. Yan, M.A. Sutton, A.P. Reynolds, Mater. Sci. Eng. A, 2004, 364, 55.
34. W.D. Lockwood, B. Tomaz, A.P. Reynolds, Mater. Sci. Eng. A, 2002, 323, 348.
35. T.J. Lienert, R.J. Grylls, J.E. Gould, H.L. Fraser, Proc. Int. Conf. on Hot deformation of aluminium alloys II, Eds. T.R. Bieler, L.A. Lalli, S.R. MacEwen, TMS, 1998, 326.
36. H.J. McQueen, S. Spigarelli, Proc. Int. Symp. Physics Materials, F Chmelik, ed., Charles Univ., Prague, 2005.
37. T. Pettersen, B. Holmedal, E. Nes, Metal. Tans., 2003, 34, 2737.
38. I. Ferreira, R.G. Stang, Acta Met., 1983, 31, 585.
39. Y. Huang, F.J. Humphreys, Acta Mater., 1997, 45, 4491.
40. Kh.A.A. Hassan, B.P. Wynne, P.B. Prangnell, FSW IV Park City Utah, 2003.
41. K.V. Jata and S.L. Semiatin, Scripta Mater., 2000, 43, 743.
42. G. Avramovic-Cingara, D.D. Perovic and H.J. McQueen, Metal. Mater. Trans. A, 1996, 27, 3478.